Available online at www.sciencedirect.com

ScienceDirect

Energy Procedia 38 (2013) 199 – 208

Energy Procedia

SiliconPV: March 25-27, 2013, Hamelin, Germany

Injection-level dependent series resistance: Comparison of CELLO and photoluminescence-based measurements

Jan-Martin Wagner, Mathias Hoppe, Andreas Schütt, Jürgen Carstensen*, Helmut Föll

Institute for Materials Sceince, Technical Faculty, Christian Albrechts University at Kiel, 24143 Kiel, Germany

Abstract

We have investigated the spatially resolved series resistance R_{ser} of multicrystalline silicon solar cells in dependence on the injection level. For the global series resistance, a variation with the injection level is known from literature. Using CELLO and photoluminescence-based R_{ser} measurements we find a qualitative change in the series resistance distribution: For low injection levels, highly recombination-active areas lead to locally increased ohmic losses; with increasing injection level, these areas become less pronounced in the R_{ser} images. This can be understood in terms of lateral currents whose strength varies with the injection level due to varying current fractions passing through the grid or being shorted by the p–n junction. A linear response-based series resistance description, comprising the variation of the series resistance with the injection level, is used to explain these findings.

Keywords: series resistance ; injection level ; luminescence-based measurements ; CELLO ; lateral voltage offsets

1. Introduction

The variation of the global series resistance (R_{ser}) of a silicon solar cell with the injection level has already been discussed before in the literature. It is related to the fact that the series resistance of a solar cell is an averaged parameter containing not only the resistivity of the silicon material and of the metallic contacts, but also (for a standard H-grid type cell) the behavior of the front-side contact network, consisting of the contact grid and the highly doped emitter. Since the emitter is directly linked to the p–n junction, the current paths through this network change as the diode forward conductivity varies along the

* Corresponding author. Tel.: +49-431-880-6181; fax: +49-431-880-6178.
E-mail address: jc@tf.uni.kiel.de

1876-6102 © 2013 The Authors. Published by Elsevier Ltd.
Selection and/or peer-review under responsibility of the scientific committee of the SiliconPV 2013 conference
doi:10.1016/j.egypro.2013.07.268

I–V curve, resulting in an injection-level dependence of the series resistance (see, e.g., [1–9]). Such variations in R_{ser} are not contained in the model of independent diodes that is widely used for the description of the local series resistance of silicon solar cells. However, for isotropic solar cells a description of injection-level dependent series resistances is possible by using the theory developed for the interpretation of CELLO [10] linear voltage response maps, taken under open-circuit condition [7].

Recently this theory was extended to luminescence-based measurements, which for appropriate measurement conditions also show a linear response behavior even for several amperes of the externally flowing current [11]. Using a sufficiently strong illumination for the luminescence-based measurements, a study of the injection-level dependence of the series resistance has been performed. Here we present such measurements, including a comparison with CELLO results. Multi-crystalline (mc) silicon cells are chosen because they show material-related intrinsic lateral currents giving rise to additional ohmic losses.

Nomenclature

CELLO	solar cell local characterization; an advanced LBIC-based solar cell measurement system
LBIC/LBIV	light beam-induced current/voltage

2. Methods for series resistance determination

2.1. CELLO measurements

CELLO is a very versatile LBIC/LBIV measurement system for solar cells. It measures (either potentiostatically or galvanostatically) the small-signal linear response to a local excitation by an amplitude-modulated laser. Since the CELLO system is time-calibrated, both amplitude and phase (time offset between excitation and response) are obtained. This enables very fast standard-LBIC-like scans (a map of about 10^6 pixels takes roughly 15 min). By applying DC light and voltage / current bias, CELLO allows to obtain maps of current or voltage response at arbitrary working points of the illuminated *I–V* characteristic. From these maps further information about the solar cell can be obtained, e.g. relative power losses occurring at maximum power point. For wafer-based silicon solar cells, a large set of electrical parameters can be determined from photo-impedance measurements (see, e.g., [12]). Also thin-film solar cells and tandem structures can be investigated by CELLO to an unprecedented degree [13–15].

The series resistance determination by CELLO measurements [7, 16, 17] is somewhat complex; its meaningfulness will be evident from the final result. It is described here in order to stress its key aspects, some of them being important physical findings in themselves. For the (illuminated) solar cell under investigation, a voltage map taken under open-circuit condition (denoted as dU_{oc} map), a current map taken under short-circuit condition (denoted as dI_{sc} map), and the corresponding illuminated *I–V* curve are needed. As an example, such maps are shown in Fig. 1 for one of the solar cells investigated in this study. The dU_{oc} map values, Fig. 1(a), decrease with increasing distance from the bus bars (where the reference electrodes are placed), and comparing this with the dI_{sc} map, Fig. 1(b), one can see that the local voltage signal scales with the locally generated photocurrent (with a scratch-like line in the left center part as an exception). Both observations are rather trivial consequences of the ohmic properties of grid and emitter. Taking the ratio between the dU_{oc} map and the dI_{sc} map takes into account the differences in the local photocurrent. The unit of measure of the resulting map is ohm, it thus is called an *R* map.

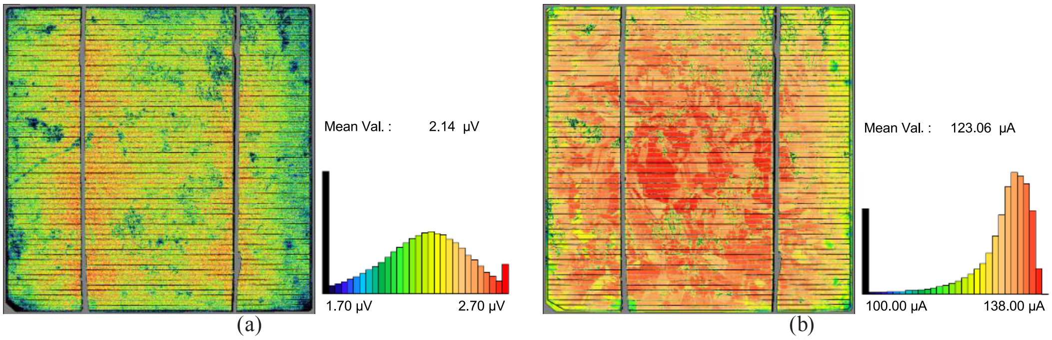

Fig. 1. CELLO maps needed for series resistance determination, here shown for an mc-Si cell: (a) voltage response under open-circuit condition (dU_{oc} map); (b) current response under short-circuit condition (dI_{sc} map)

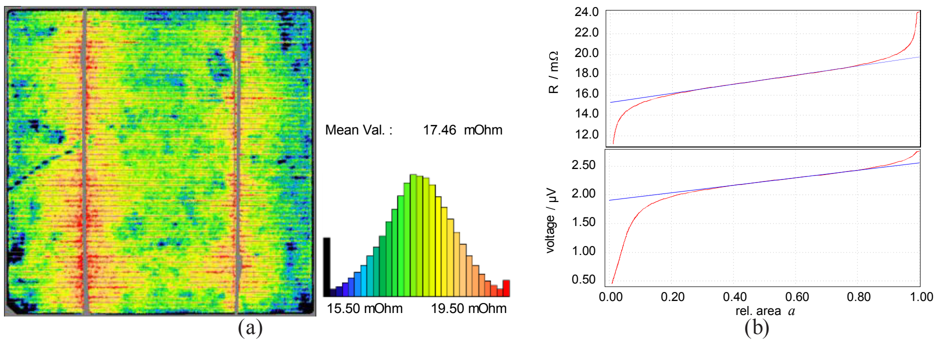

Fig. 2. (a) CELLO R map ($= dU_{oc} / dI_{sc}$) obtained from Fig. 1 (smoothed); (b) upper graph: corresponding distribution of the R map values over the relative area a of the solar cell (red curve), with a straight line fitted to the central part (blue curve); lower graph: ditto for the dU_{oc} map values of Fig. 1(a)

To extract the series resistance information from the R map, the distribution of its values over the solar cell area is considered, which is obtained from the integral $N(R) := \int_0^R H(R')\mathrm{d}R'$ over the corresponding histogram data, $H(R)$. Normalizing $N(R)$, the number of pixels having a map value $\leq R$, to the total number of pixels by defining $a(R) := N(R) / N(\infty)$, represents the relative area of the solar cell having map values $\leq R$. The inverse function $R(a)$ gives the distribution of the R values over the solar cell area. The R map obtained from both maps of Fig. 1 is shown in Fig. 2(a), with the corresponding $R(a)$ distribution being shown in Fig. 2(b) (upper graph). It exhibits a typical behavior, being a linear curve over a large part of the relative solar cell area; only for the smallest and the largest R values it deviates from a straight line. From our experience, this holds for all “economically reasonable” solar cells [16]. As will be seen below, a linear distribution is an important prerequisite for the definition of a local series resistance map. The linear variation of the R values over the (relative) area of the solar cell means that for a hypothetically homogeneous photocurrent production the resulting photovoltage distribution over the area of the solar cell would be linear too. In practice, however, if the solar cell exhibits a non-homogeneous but isotropic photocurrent production, still a linear voltage distribution is found (i.e., a constant lifetime is not necessary; however, strong inhomogeneities like, e.g., a massive agglomeration of sites with very low photocurrent might be critical). This is shown in Fig. 2(b) (lower graph) for comparison.

The meaning of the term “series resistance” is basically known from the global equivalent circuit of a solar cell as found in any textbook. In a CELLO measurement, small-signal linear response conditions hold, therefore the corresponding global equivalent circuit can be simplified [16]. An ohmic resistor R_d, with a value that varies along the I–V curve, represents the ideal diode. R_d is simply the differential resistance (i.e., the reciprocal slope) of the ideal diode characteristic. Then, neglecting shunts, the total solar cell resistance (i.e. the differential resistance of the global I–V characteristic at the working point used in the small-signal linear response measurement) is just the sum of global series and diode resistance: $R_{sc} = R_{ser} + R_d$. This relation is used as a starting point for the definition of local series resistance values as follows. The linear $R(a)$ distribution discussed above can be described by a simple solar cell model [7], being analytically solvable in the small-signal linear response regime and just representing very general features of the resistance behavior of a solar cell. In this model, the average of $R(a)$ equals the global R_d value, $\langle R(a)\rangle = R_d$, and the maximum of the R values equals R_{sc}. From the linear-response equivalent circuit one learns that $R_{ser} = R_{sc} - R_d$, and this allows to introduce a relative-area-dependent series resistance function by defining $R_{ser}(a) := R_{max} - R(a)$. This definition has two important consequences which justify the choice for $R_{ser}(a)$: (i) Due to $R(a)$ being a linear distribution, also $R_{ser}(a) = R_{max} - R(a)$ is a linear distribution, which allows a simple arithmetic averaging of $R_{ser}(a)$, and (ii) the arithmetic average of $R_{ser}(a)$ fulfills exactly the relationship of the linear-response equivalent circuit:

$$\langle R_{ser}(a)\rangle = \langle R_{max} - R(a)\rangle = R_{max} - \langle R(a)\rangle = R_{sc} - R_d = R_{ser}\,. \tag{1}$$

It has to be emphasized that only by this correspondence to the equivalent circuit it makes sense to define $R_{ser}(a)$ values *at all*, and that this correspondence only holds due to the linear behavior of $R(a)$. Without a linear $R(a)$ distribution, $R_{ser}(a)$ cannot be defined in a meaningful way, since then there is no averaging rule enabling the necessary link to the global R_{ser} value – i.e. to where the meaning of "series resistance" comes from. Finally, in an analogous way, the map of local R_{ser} values is defined; this map has the same arithmetic averaging properties as just discussed for $R_{ser}(a)$:

$$R_{ser}(x, y) = R_{max} - R(x, y)\,. \tag{2}$$

The correct absolute values of the $R_{ser}(x, y)$ map depend crucially on taking the correct difference in (2). This can be troublesome due to noise in the data, which may make it hard to identify R_{max} with sufficient accuracy. Rescaling the R_{ser} map so that it reproduces the correct global R_{ser} value as obtained from a fit to the illuminated I–V curve solves this problem. This fit takes into account that R_{ser} varies along the I–V curve [17], which is a further result obtained from the above-mentioned simple solar cell model. This is so because the distributed part of the global series resistance depends on the diode resistance and therefore varies with the injection level (or, equivalently, with the voltage U, which can be understood as the diode voltage in the equivalent circuit) [7] according to

$$\frac{1}{R_{ser}^{distr}(U)} = \frac{1}{R_{ser}^{\infty}} + \frac{1}{R_d(U)}\,. \tag{3}$$

The series resistance map resulting from Fig. 2(a) by applying the procedure described above is shown in Fig. 3(a), slightly smoothed to reduce the noise, and the corresponding $R_{ser}(a)$ distribution is shown in Fig. 3(b). The deviations from the straight line for the smallest and the largest R_{ser} values can be understood as (i) influence of contact resistances not included in the underlying model and (ii) deviations from the purely two-dimensional current flow holding in the underlying model for the whole solar cell area [7] but which obviously cannot hold next to the edge and to the main bus bars, where current flow is mainly one-dimensional. Further general features of this map will be discussed in the results section.

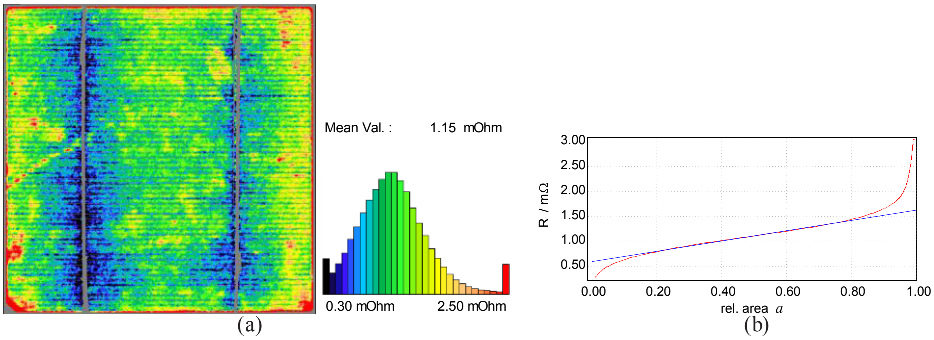

Fig. 3. (a) CELLO R_{ser} map obtained from Fig. 2(a) (smoothed); (b) distribution of the R_{ser} map values over the relative area a of the solar cell (red curve), with a straight line fitted to the central part (blue curve)

2.2. Photoluminescence-based measurements

For the determination of the spatially resolved series resistance from luminescence measurements, recently a newly developed model was introduced [11] that allows a linear response analysis analogous to the procedure described above for CELLO measurements. This model is briefly reviewed here. For a given illumination strength, consider the lateral voltage distribution U that due to an externally flowing current I_{ext} deviates from the corresponding one under open-circuit condition, U_0:

$$U(x, y, I_{ext}) = U_0(x, y) + R(x, y)\, I_{ext}. \qquad (4)$$

$R(x, y)$ is the total resistance, it corresponds to the R map of CELLO. For currents entering (leaving) the solar cell, one has $I_{ext} > 0$ ($I_{ext} < 0$). Obviously, equ. (4) also holds for an idealized grid with zero series resistance; then, R equals the diode resistance. For a finite series resistance a potential difference, denoted as U_{ser}, occurs between the external contact (reference electrode, index e) and any local position. Up to linear order, this potential difference can be written as

$$U_{ser}(x, y, I_{ext}) = [R(x_e, y_e) - R(x, y)]\, I_{ext} =: R_{ser}(x, y)\, I_{ext}. \qquad (5)$$

Notice that dark currents flowing locally through the diode do not play any role for the definition of a local series resistance. From the continuity equation and Ohm's law for the lateral currents in the emitter it follows that the local diode current determines the local Laplacian of the potential (see, e.g., [18]). All local series resistance properties of the solar cell are contained in $U(x, y, I_{ext})$ and are therefore captured by $R_{ser}(x, y)$, as defined in (5), up to the linear order.

For a valid application of this theory the linearization in (4) must hold. The diode characteristic of the p–n junction introduces an unavoidable nonlinearity, and since R is related to the diode resistance, care must be taken. Since the external current is given by $I_{ext} = I_d - I_{ph}$, with the total dark (i.e., diode) current I_d and the photocurrent I_{ph}, the influence of the diode nonlinearity can be minimized for given external current by adjusting the photocurrent (via the illumination intensity) to fulfill the condition

$$I_{ext} + I_{ph} = I_d = \text{const.} \qquad (6)$$

Since (5) is linear, R_{ser} can be determined from a variation in U_{ser} resulting from a variation in I_{ext}. To that end, two luminescence images M_1 and M_2, corresponding to the external currents I_1 and I_2, can be taken for different loads, with the external current adjusted so that M_1 and M_2 have the same average value, which is more or less equivalent to fulfilling (6). From these images, first an R-like image is calculated according to $R(x, y) = kT \ln(M_2 / M_1)/ (q\, \Delta I)$, with $\Delta I = I_2 - I_1$. The histogram data of this image can be used to check for the required linear distribution. As for CELLO, the series resistance image is obtained as $R_{ser}(x, y) = R_{max} - R(x, y)$. Typically, the first luminescence image (M_1) is taken under current extraction ($I_{ext} < 0$), and the second (M_2) under open-circuit condition with reduced illumination strength according to (6). Another possibility is to use a fully contact-less measurement principle (ShaLum: shaded luminescence [11, 19]), which so far provides only qualitative series resistance images. For the present work, however, this isn't a drawback since here we focus on the qualitative changes in series resistance when varying the injection level. ShaLum is based on a systematic inhomogeneous illumination of the solar cell, e.g. by shading half of its area, thereby generating lateral currents of the same type as if the cell were contacted and current taken out. An open-circuit image of the whole cell is used as M_1, and a sum image of two shading situations is taken as M_2 in the above-described procedure. Estimating the lateral current flowing for the sum image (by comparison with an image obtained under current extraction), roughly the same order of magnitude for R_{ser} is found as for the CELLO map, Fig. 3.

In luminescence measurements, much larger currents (amperes) are used than for CELLO (sub-milliamps). Therefore it is not *a priori* clear that in such a luminescence measurement the solar cell shows linear response behavior. In all the measurements done so far in our group it turned out that this is the case even for several amps of external current: The strength of the voltage variation showed a linear scaling with the external current. This is interpreted according to (5) as ohmic resistance behavior.

3. Experiments and results

We have investigated various kinds of mc-Si solar cells, all showing the behavior presented below for a few exemplarily chosen cells (of size 12.5 × 12.5 cm^2; fabricated for research purposes in a standard industrial process). The CELLO measurements have been performed under a global illumination of about 1/3 sun, all maps presented here have been taken with an infrared laser (wavelength 830 nm). For the contacting of the cell (current leads), novel bar electrodes have been used. To avoid the distorting influence of shading by electrical contacts, for the photoluminescence (PL) measurements the ShaLum technique has been used. Illumination strengths of 2/3, 1, and 4/3 sun have been used on the non-shaded parts and lower intensities for the open-circuit image of the whole cell, determining the effective injection level. For ShaLum, the bus bars have not been reinforced in order to increase their conductivity. All R_{ser} images shown have been checked to exhibit a mainly linear $R(a)$ distribution (not explicitly shown).

3.1. Sample cell A: bad edge region perpendicular to the bus bars

Figure 4 shows CELLO dI_{sc} and R_{ser} maps of a cell that has several strongly recombination-active grains close to its upper edge, and the whole upper-edge region of 2 cm width shows a reduced photocurrent generation. Overall, the R_{ser} map shows the lowest values close to the bus bars, as expected. However, the highest values are found at places with reduced photocurrent generation (the whole upper edge region as well as strongly recombination-active sites, except for those lying adjacent to the bus bars). Additionally, a laser-scribed mark at the lower edge of this cell leads to high values in the R_{ser} map. Figure 5 shows series resistance images of the same cell obtained by ShaLum. Taken for lowest injection, Fig. 5(a) is quite comparable to the CELLO R_{ser} map concerning the influence of the strongly recombination-active sites. Systematic differences between Fig. 4(b) and Fig. 5(a) are found for the upper edge region (reduced series resistance in the ShaLum image), for the area between the bus bars (increased values in the ShaLum image), and for the laser-scribed mark (less pronounced in the ShaLum image).

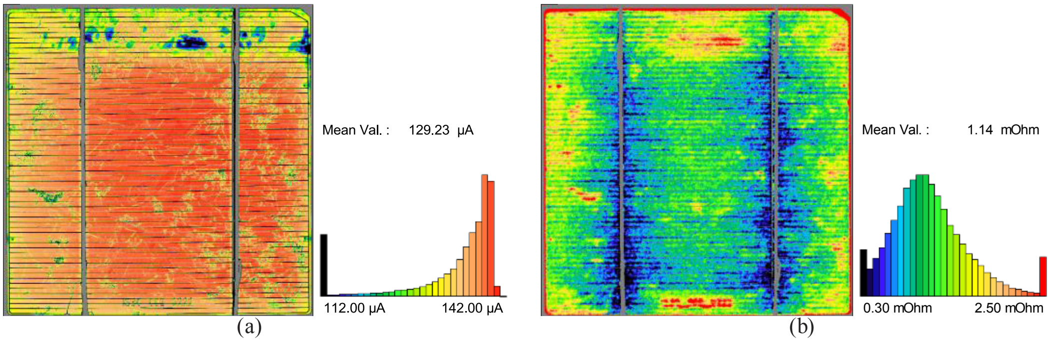

Fig. 4. CELLO results for sample cell A: (a) dI_{sc} map; (b) R_{ser} map (smoothed)

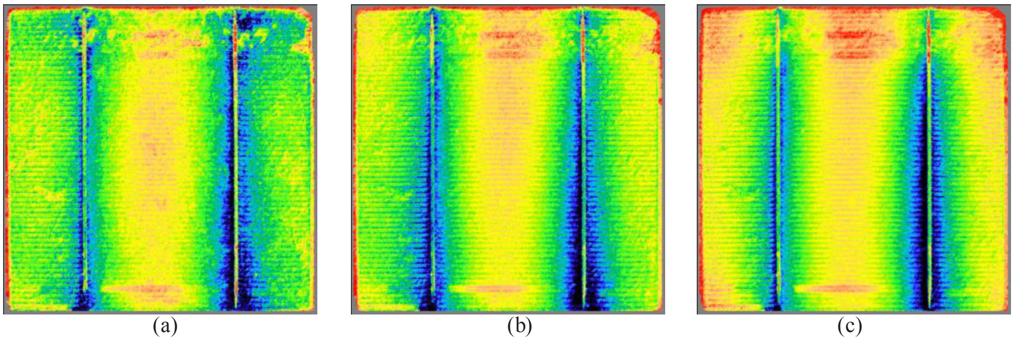

Fig. 5. ShaLum R_{ser} images (qualitative: each image separately scaled between zero and its maximum, the latter decreasing for increasing injection level) of sample cell A for various effective injection levels (all images smoothed): (a) approx. 2/5 sun; (b) approx. 3/5 sun; (c) approx. 4/5 sun

For increasing injection level, the ShaLum images show qualitative changes: Most of the strongly recombination-active sites and the laser-scribe mark become less pronounced, the upper edge region becomes more pronounced, and a few rectangular features of increased series resistance appear which most probably are due to broken grid fingers.

3.2. Sample cell B: bad edge region parallel to the bus bars

Figure 6 shows CELLO dI_{sc} and R_{ser} maps of a cell that has several strongly recombination-active grains close to its right edge, and the whole right-edge region shows reduced photocurrent generation in a width of about 2 cm. The R_{ser} map again shows the lowest values close to the bus bars, and the highest values result either from places with reduced photocurrent generation (the whole right-edge region as well as strongly recombination-active sites), from broken grid fingers, or from the laser-scribe mark at the right edge of this cell. Figure 7 shows series resistance images of the same cell obtained by ShaLum. Taken for lowest injection, Fig. 7(a) shows detailed similarities to the CELLO R_{ser} map concerning the influence of the strongly recombination-active sites. Systematic differences between Fig. 6(b) and Fig. 7(a) are found for the relative strength of the recombination-active sites on the right-edge region and elsewhere on the solar cell (large difference for ShaLum), for the area between the bus bars (increased values in the ShaLum image), and for the laser-scribed mark (practically absent for ShaLum).

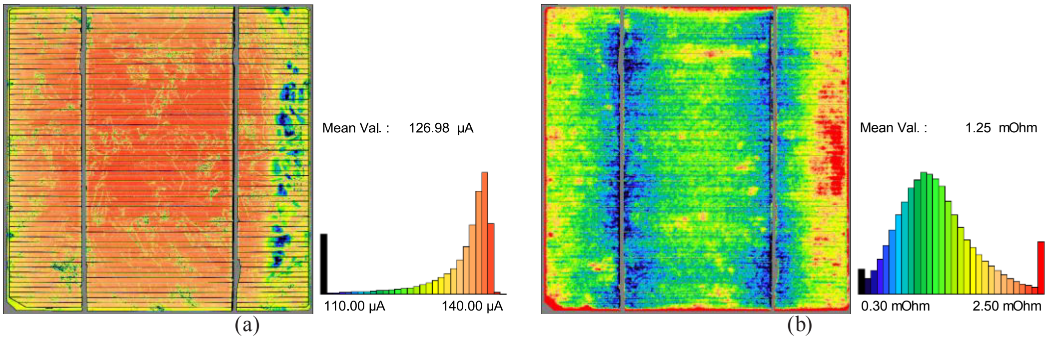

Fig. 6. CELLO results for sample cell B: (a) dI_{sc} map; (b) R_{ser} map (smoothed)

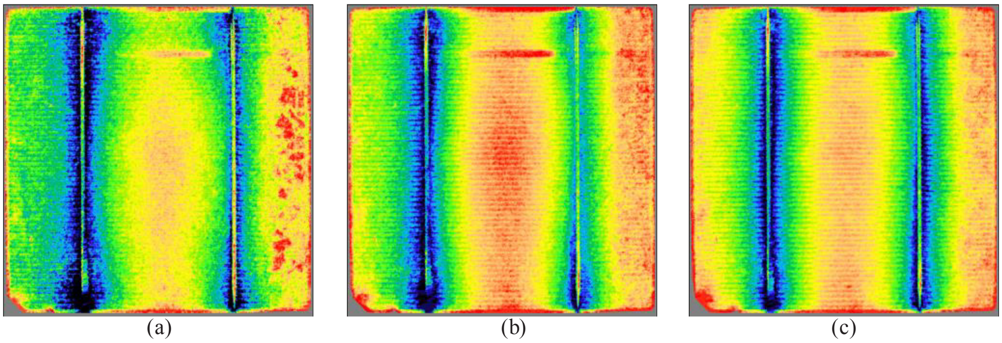

Fig. 7. ShaLum R_{ser} images (qualitative: each image separately scaled between zero and its maximum, the latter decreasing for increasing injection level) of sample cell B for various effective injection levels (all images smoothed): (a) approx. 2/5 sun; (b) approx. 3/5 sun; (c) approx. 4/5 sun

For increasing injection level, the ShaLum images show qualitative changes: Most of the strongly recombination-active sites become less pronounced, and the three cell parts as divided by the bus bars become nearly equally pronounced; a few broken grid fingers are visible for all injection levels.

4. Discussion

A common feature of all presented low-level injection series resistance maps/images is that sites of significantly reduced photocurrent production show increased R_{ser} values. This is due to currents flowing laterally into the emitter, driven by differences in local photocurrent production. Flowing through a grid with finite series resistance, these equilibrating lateral currents may cause internal voltage offsets leading to local ohmic losses or, equivalently, effectively increased local series resistance. Recombination-active sites lying adjacent to the bus bars (cf. upper edge region of cell A) show a weaker effect since for currents to reach them from the bus bars, the series resistance is much smaller; such sites are “fed” quite easily with current collected from the bus bars, i.e. without causing large voltage offsets.

The qualitative change of the ShaLum series resistance images concerning the visibility of the strongly recombination-active sites for varying injection level can be understood from the injection-level dependence of the distributed part of the series resistance itself, as expressed by (3). Descriptively, (3) represents parallel paths for the current: to pass through the grid or to become shorted by the diode. For increasing injection level, R_d becomes smaller, which means that lateral currents can be more easily shorted by the diode. Thereby, R_{ser} is effectively reduced at higher injection, which is the reason for the decreasing maximum value of the ShaLum images. As a consequence, the equilibrating lateral currents lead to smaller internal voltage offsets, i.e. to reduced ohmic losses related to highly recombination-active areas. This can be interpreted as that equilibrating currents are preferentially shorted. It follows that there are different lateral current flow types, reacting differently to the switching-on of the diode: Equilibrating currents belonging to large locally increased ohmic losses are shorted while currents following the technically preferred paths, having smaller series resistances, are much less affected.

Note that in the model of independent diodes, constant ohmic resistors describe the local series resistances, and lateral equilibrating currents are not taken into account. Therefore, the model of independent diodes cannot describe the observed effects.

There are several observations related to the ShaLum series resistance images not discussed so far: the deviating behavior of the upper edge region of sample cell A, of the cell section between the bus bars (for both sample cells), the visibility of the laser-scribed mark, and the strongly varying visibility of recombination-active sites on sample cell B. There are strong hints that they are all related to intrinsic injection-level dependencies of the bulk lifetimes in the relevant regions of the cells. Calculating ratio images of the open-circuit PL images taken for different illumination strengths reveals significant inhomogeneities, with the center area between the bus bars behaving differently than the outer parts and the laser-scribed mark as well as the "bad" edge regions showing further deviating behavior. In addition, due to the inhomogeneities introduced by the bad edge regions, it cannot be ensured that (6) holds in every region of the solar cell, therefore an influence of the diode nonlinearity cannot be excluded. Nevertheless, even when using two electroluminescence images for calculating a series resistance image, a qualitatively correct result is obtained. Therefore, all ShaLum images discussed can still be considered to be reasonable series resistance images. Yet all this is related to special properties of the specific sample cells and is therefore not instructive regarding the general injection-level dependent behavior of the series resistance. Still, it is decisive for understanding the ShaLum measurement method. However, this was not in the focus of the present paper but will be dealt with separately.

5. Summary and conclusions

We have investigated mc-Si solar cells having strongly recombination-active regions that lead to internal equilibrating currents flowing laterally in the emitter. In some cell areas these internal currents are so large that they cause increased ohmic losses noticeable in spatially resolved series resistance measurements. It is found that the strength of these losses varies: For increasing injection level, they become smaller. This can be understood by the injection-level dependence of the series resistance caused by the diode effectively forming a parallel connection to the current path through grid and emitter. Then, an increasing current fraction can be shorted by the diode due to its reduced resistance for increasing injection level. Altogether, our results show that (i) CELLO and luminescence measurements complement each other in that CELLO can analyze very well the low-injection regime, while luminescence measurements allow to gain insight for higher injection levels; (ii) injection-level dependent spatially resolved series resistance measurements can be used to distinguish certain contributions to R_{ser}; and (iii) technologically relevant series resistance problems show up most pronounced at high injection levels.

Acknowledgements

This work was supported by the DFG (German Research Foundation) under grant FO 258/11-2.

References

[1] Wolf M, Rauschenbach H. Series resistance effects on solar cell measurements. *Advanced Energy Conversion* 1963;**3**:455–79.

[2] Dhariwal SR, Mittal S, Mathur RK. Theory for voltage dependent series resistance in silicon solar cells. *Solid-State Electronics* 1984;**27**:267–73.

[3] Bhattacharya DK, Mansingh A, Swarup P. Dependence of series resistance on operating current in p-n junction solar cells. *Solar Cells* 1986;**18**:153–62.

[4] Araújo GL, Cuevas A, Ruiz JM. The effect of distributed series resistance on the dark and illuminated current–voltage characteristics of solar cells. *IEEE Transactions on Electron Devices* 1986;**33**:391–401.

[5] Altermatt PP, Heiser G, Aberle AG, Wang A, Zhao J, Robinson SJ, et al. Spatially resolved analysis and minimization of resistive losses in high-efficiency Si solar cells. *Progress in Photovoltaics: Research and Applications* 1996;**4**:399–414.

[6] Bowden S, Rohatgi A. Rapid and accurate determination of series resistance and fill factor losses in industrial silicon solar cells. In: *Proc. 17th European Photovoltaic Solar Energy Conference* 2001 (Munich, Germany), pp. 1802–6.

[7] Carstensen J, Schütt A, Föll H. CELLO local solar cell resistance maps: modeling of data and correlation to solar cell efficiency. In: *Proceedings of the 22nd European Photovoltaic Solar Energy Conference* 2007 (Milan, Italy), pp. 337–40.

[8] Fong KC, McIntosh KR, Blakers AW. Accurate series resistance measurement of solar cells. *Progress in Photovoltaics: Research and Applications*, DOI: 10.1002/pip.1216

[9] Breitenstein O, Rißland S. A two-diode model regarding the distributed series resistance. *Solar Energy Materials & Solar Cells* 2013;**110**:77–86.

[10] Carstensen J, Popkirov G, Bahr J, Föll H. CELLO: an advanced LBIC measurement technique for solar cell local characterization. *Solar Energy Materials & Solar Cells* 2003;**76**: 599–611.

[11] Wagner J-M, Carstensen J, Berhane A, Schütt A, Föll H. Series resistance analysis with the shaded luminescence technique. In: *Proceedings of the 26th European Photovoltaic Solar Energy Conference* 2011 (Hamburg, Germany), pp. 1569–75.

[12] Carstensen J, Schütt A, Popkirov G, Föll H. CELLO measurement technique for local identification and characterization of various types of solar cell defects. *Physica Status Solidi C* 2011;**8**:1342–6.

[13] Nguyen M, Stegmaier M, Schütt A, Carstensen J, Föll H. The influence of the electrode sheet resistance on local photocurrent exitations in microcrystalline Silicon thin film solar cells. In: *Proceedings of the 27th European Photovoltaic Solar Energy Conference* 2012 (Frankfurt, Germany), pp. 2590–3.

[14] Schütt A, Carstensen J, Wagner J-M, Föll H, Nguyen M, Klein S. Spectrally resolved local CELLO characterization of tandem solar cells using linear and 2nd harmonic response analysis. In: *Proceedings of the 27th European Photovoltaic Solar Energy Conference* 2012 (Frankfurt, Germany), pp. 2598–603.

[15] Wagner J-M, Carstensen J, Schütt A, Föll H. Qualitative and quantitative evaluation of thin-film solar cells using solar cell local characterization. *Journal of Applied Physics* 2013;**113**:064503.

[16] Carstensen J, Schütt A, Föll H. Modelling of the distributed series grid resistance: verification by CELLO measurements and generalization to other resistance mapping tools. In: *Proceedings of the 23rd European Photovoltaic Solar Energy Conference* 2008 (Valencia, Spain), pp. 338–41.

[17] Carstensen J, Abdollahinia A, Schütt A, Föll H. Characterization of the grid design by fitting of the distributed series grid resistance to CELLO resistance maps and global IV curves. In: *Proceedings of the 24th European Photovoltaic Solar Energy Conference* 2009 (Hamburg, Germany), pp. 516–19.

[18] Glatthaar M, Haunschild J, Zeidler R, Demant M, Greulich J, Michl B, et al. Evaluating luminescence based voltage images of silicon solar cells. *Journal of Applied Physics* 2010;**108**:014501.

[19] Carstensen J, Schütt A, Föll H, Warta W, Kasemann M. Measuring method and device for characterizing a semiconductor component, European Patent EP 2 245 473 B1; 2012.